Hindawi
Complexity
Volume 2019, Article ID 3765821, 11 pages
https://doi.org/10.1155/2019/3765821

Research Article

Variable Speed Pump Storage for the Mitigation of SSR in Power System with Wind Generation

Ye Fengchun,[1] Girmaw Teshager Bitew ,[2] Han Minxiao ,[2] Sun Yao,[2] and Zhang Hanhua[1]

[1]*Electric Power Research Institute, State Grid Ningxia Electric Power Co., Ltd., Yinchuan, China*
[2]*School of Electrical Engineering, State Key Laboratory of Alternate Electrical Power System with Renewable Energy Sources, North China Electric Power University, Beijing 102206, China*

Correspondence should be addressed to Han Minxiao; ncepu_vsc@163.com

Received 2 July 2019; Accepted 23 August 2019; Published 10 December 2019

Guest Editor: Xiaoqing Bai

Subsynchronous resonance (SSR) can bring significant negative effects on the grid system like stability, security, and even generator shaft damage. This work presents a new method of using a doubly-fed induction machine (DFIM) based system of variable speed pumped storage plant (VSPS) to mitigate SSR in the power system with high penetration of wind generation. The mitigation is reached based on the principle of balanced shaft mechanical input power and electromagnetic power. The fundamental concepts and phenomena of SSR with wind farm are discussed in brief in this work. For the sake of analysis and verification of performance of the proposed system, the network model including wind farm, VSPS, HVDC, and synchronous machine is built based on Ningxia grid for the SSR study using PSCAD platform. The result shows that VSPS brings significant effect to dampen the SSR in the power system with high penetration of wind generation.

1. Introduction

Subsynchronous resonance (SSR) in a power system is an electromechanical instability occurrence when the interaction exists between the torsional modes of generator shafts and effect of series-compensated transmission line running with less than the nominal grid frequency [1]. The studies have also confirmed that the wind farms constructed with doubly-fed induction generator (DFIG) and connected to series capacitor compensated transmission lines are quite vulnerable to subsynchronous interaction (SSI) and cause the escalation of SSR in the power system. SSR brings significant negative effects on the grid system like stability, security, and even generator shaft damage [2, 3]. So, the analysis and mitigation for SSR is imperative.

There are two categories in practice to mitigate SSR: one is primary machine parameters modification and the other one is the secondary control loop [4, 5]. The typical examples for the first one are pole-face amortisseur windings at the generator rotor, blocking filter, TCSC, NGH damper, phase shifters, static var compensator (SVC), etc. The most typical example of the second one is using generator excitation regulator. In addition, different supplementary damping measures of FACTS have been put forward in [6–8]. Besides, to mitigate SSR, a new method of using a doubly-fed induction machine (DFIM) based system of variable speed pumped storage plant (VSPS) is proposed based on the principle of balanced shaft mechanical input power and electromagnetic power. Electromagnetic power can be calculated by the power flow of DFIM terminal to the grid, and thus controlled by the converters connected to the DFIM. By regulating injecting or absorbing active power of DFIM according to the generator speed deviation, the balance of the shaft power will be maintained smooth; therefore, VSPS can provide damping for SSR and suppress transient torque amplification effect. Regulating the absorbing or generating reactive power by the converters of the VSPS also keeps the AC voltage oscillations damped quickly. To analyse SSR and validate the performance of the proposed system, the network model including wind farm, VSPS, HVDC, and synchronous machine is built based on Ningxia grid for the study of SSR using PSCAD platform.

2. Problem Description Associated with Wind Generation

The SSR of DFIG originates from the resonance of the inductance-capacitance (L-C) of the components, but is reinforced by the converter control of DFIG. The latter, by greatly enlarging the negative resistance at the slip frequency, serves as the primary reason for the self-excitation of SSR, even under the context of a very low series compensation. This has been explained by theoretical analysis and confirmed by field observations [6]. It would significantly increase the absolute value of the negative resistance and thus contribute a lot to an unstable oscillation [2]. Consequently, DFIG is made much more vulnerable to the subsynchronous control interaction (SSCI)-type SSR. SSCI is emerged that there is a growing risk of SSR caused by the interaction between DFIGs and series compensated transmission line due to the increasing applications of wind power energy and series compensation.

In the SSR event, the frequency at different locations is identical, meaning all wind turbine generators (WTGs) and the network are engaged in the same SSR mode. But its value is not fixed and keeps changing over time as well as the variation of the factors such as the network topology and number of online generators [6].

According to the study of [7], many SSR phenomena have been detected in Guyuan, Hebei in 2010. The current of both DFIG of the wind farm and transmission line oscillates with large magnitude at the subsynchronous frequency.

The proposed system in this paper is designed based on the IEEE second benchmark model of SSR so that the SSR can be well analysed. This wind generator model is shown in (Figure 1). An equivalent lumped machine is provided to represent a behaviour of a group of wind turbines. As many studies [11, 12] support this assumption, the aggregation of a wind farm provides a reasonable approximation for system interconnection studies. According to system studies [13–16], simulations of bulk system dynamics using a single machine equivalent is adequate for most planning studies.

Based on this lumped wind machine model, the system shown in (Figure 2) is considered for the case study for Ningxia grid that consists of large penetration of wind and PV generation with HVDC sending out. The synchronous machine mechanical system of the model consists of exciter, generator, low-pressure (LP) and high-pressure (HP) turbine sections. PSCAD model is built for Figure 2 for the case study and the detailed analysis is presented in the following section.

The effect of SSR is also distributed into the grid. The following Figures including Figures 3–5 show the effect of SSR on the voltage, power flow and speed responses of wind farm, and HVDC operations.

While the synchronous generator is connected to the infinite bus AC-source, the operation is responding very well. But, when the infinite bus AC-source is shunted by RL components, the SSR starts due to the dominant effect of the series capacitor which is interacted with the torsional shaft mode of operation of the generator.

The transition time is made at $t = 1.5$ seconds. The RL remains connected for 0.2 s. However, even if the RL is disconnected, the resonance and the disturbance continue as in Figure 4.

The effects of SSR in the power grid considered in Figure 5 are presented in the simulated waveforms shown in the following Figures.

It can be concluded that the SSR has significant effect on the quality of voltage and power flow of the grid. It is more pronounced on the proximity where SSR is emerged. It leads to system failure and is a threat of power security. Thus, it needs to be suppressed by the appropriate method or technique. Some methods used so far have been presented in the introduction section in this paper. Besides, a new method of using a doubly-fed induction machine (DFIM) based system of variable speed pumped storage plant (VSPS) to mitigate SSR is proposed in this paper and discussed in the following section.

3. VSPS for the Mitigation of the SSR

The VSPS plays important roles in the power grid for its energy management, stability control and renewable energy resources smoothening. If it deploys a DFIM topology, it is very suitable in independent and fast active and reactive power controls. Another advantage includes that the speed of the machine is no longer locked to system frequency. Thus, in the steady state, the controls select the optimum relationship between gate position and speed to get the desired power. Hence, the efficiency and the operation flexibility of the conventional pumped storage running at constant speed can be noticeably increased by using variable speed groups. The VSPS, in general, has an immense advantages and benefits for wind power fluctuation compensation and other renewable energy smoothening, stability control, frequency control, and AC voltage control among others. Thus, it is suitable and verified that this new method of using a doubly-fed induction machine (DFIM) based system of variable speed pumped storage (VSPS) is capable of mitigating the SSR based on the principle of power balance between the machine shaft power and electromagnetic power, which is regulated by the VSPS control strategy. The electromagnetic power can be calculated by the equivalent power flow of the VSPS in to the grid, and thus regulated by the converters connected to in the DFIM. The structure of the recommended system is illustrated with a single-line diagram shown in (Figure 6). The VSPS power is defined by (1) under $d-q$ frame.

$$P_s = \frac{3}{2}\left(v_{qs}i_{qs} + v_{ds}i_{ds}\right),$$
$$Q_s = \frac{3}{2}\left(v_{qs}i_{ds} - v_{ds}i_{qs}\right), \tag{1}$$

where P_s, Q_s, v_{dqs} and i_{dqs}, are, respectively, active power, reactive power, dq-axis voltages, and dq-axis currents of the stator terminal of the DFIM.

According to [12], the VSPS is very effective for regulating grid frequency and AC voltage, stability control and wind power compensation as it is proved and verified with the case study end experimental results. By regulating injecting or absorbing active power of DFIM, the balance of the power in the grid will be maintained. Regulating the absorbing or

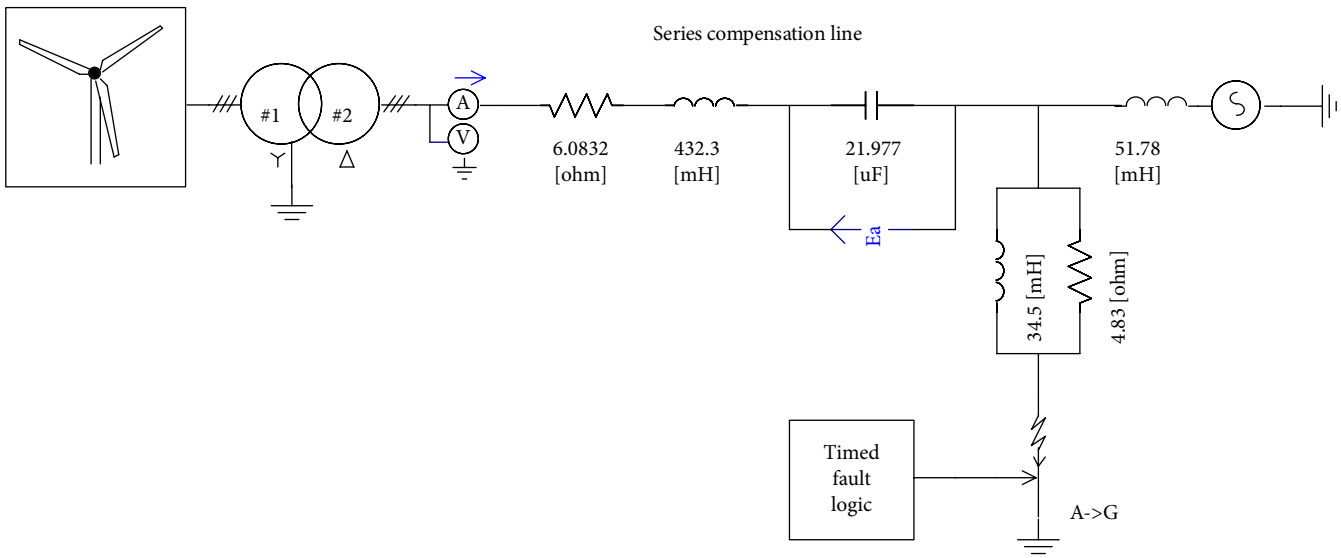

Figure 1: The PSCAD circuit diagram model of wind farm built based on IEEE second benchmark circuit model.

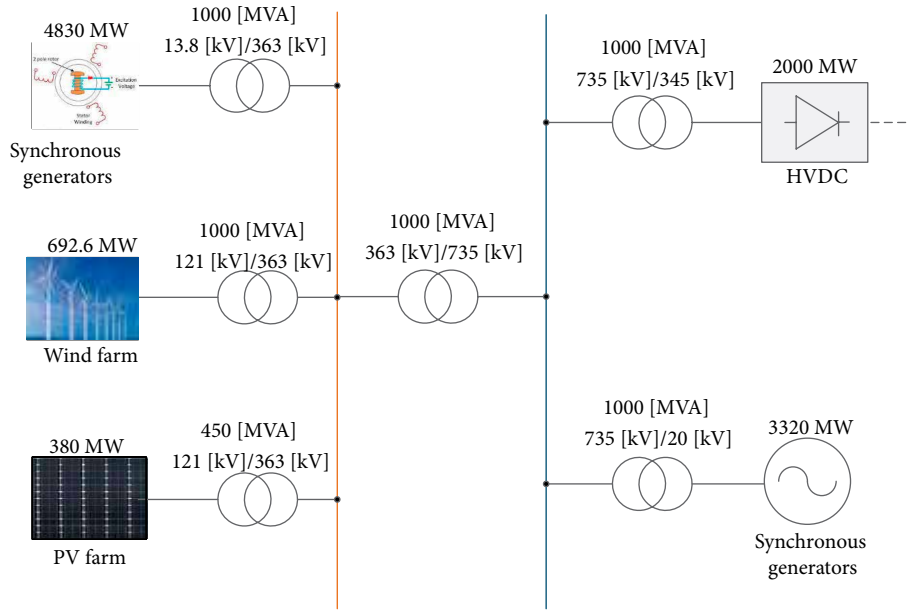

Figure 2: The structure of the power grid to study SSR, its effect, characteristics.

generating reactive power by the converters of the VSPS also keeps the AC voltage oscillations damped quickly. Therefore, this principle brings a balanced shaft mechanical input power and electromagnetic power, which is able to suppress the SSR very quickly. Hence, VSPS can provide damping for SSR and suppress transient torque amplification effect. To analyse SSR and validate the performance of the proposed system, IEEE second benchmark model of SSR is used.

Based on the basic theoretical description of the VSPS DFIM presented in (1), (2), and (3), flexible and fast control strategy is likely possible to design for mitigating the SSR in the power system. Since VSC allows the DFIM more versatile and flexible for controlling, the VSC system is a preferable option and used in this study. Basically, two main methods including voltage-mode control and current-mode control exist for controlling active and reactive power in the VSC system. In a voltage-mode control, there is no control loop closed on the VSC line current. As a result, the VSC is not protected against over-currents, whereas, in the current-mode control, the VSC line current is tightly regulated by a dedicated current-control scheme. In this study, thus, current-mode control strategy is employed for controlling the real and reactive power that each VSC system exchanges with the corresponding AC system. The VSC also allows to adopt the droop control mounted on the PQ-control. The control design is presented in the following section.

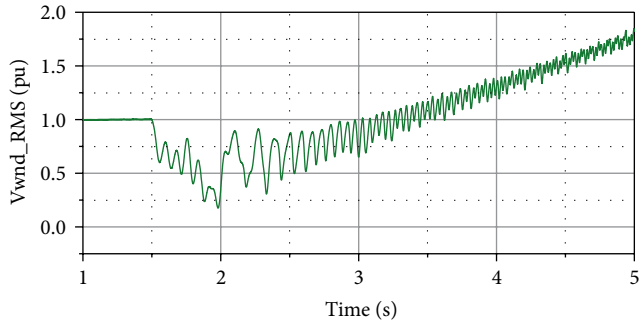

Figure 3: The wind farm machine terminal AC voltage characteristics.

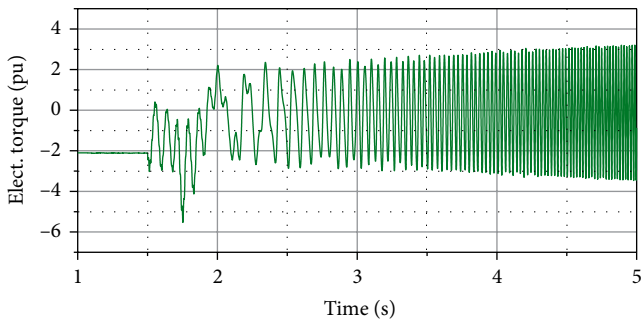

Figure 4: Electrical torque characteristics due to SSR in the wind farm.

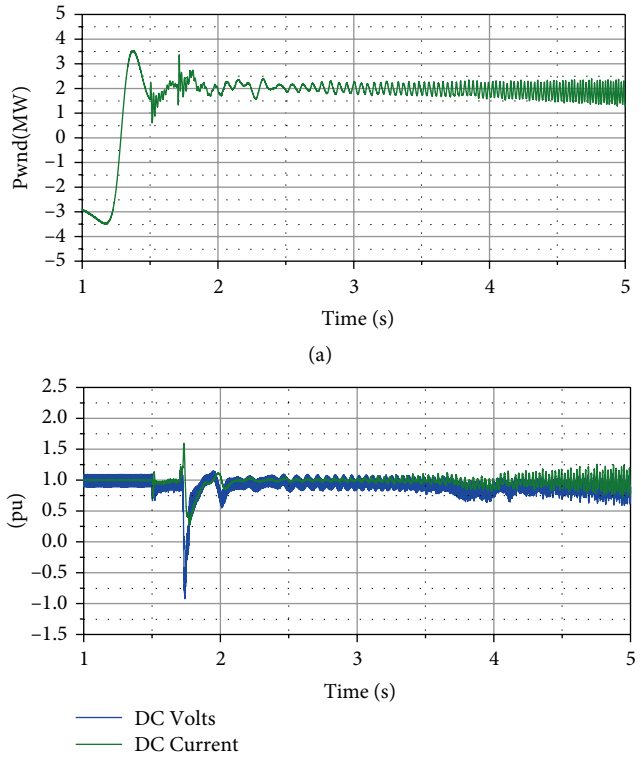

Figure 5: Effect of SSR in the grid. (a) Power flow in one of the wind farm turbines. (b) DC voltage and current responses in the HVDC.

4. Control Design of the VSPS

4.1. VSC Based DFIM Control. The hierarchical control structure (the current controllers in the inner loops and the active/reactive power control in the outer loops) of VSC based DFIM topology is implemented in this study for its effectiveness. To minimize the excursions of the grid frequency and AC voltage deviations caused by the contingencies, the outer loop control of the rotor side converter (RSC) is supported by the droop control. (Figure 7) illustrates the control structure proposed in this study. The droop control scheme is vested on the control strategy. Direct power control is an extension of direct torque control, which is a vector control family. In the implementation of direct power control, control of the instantaneous real and reactive power is independent, simple, and direct. In the application of VSPS, this type of control scheme attempts to assure having lower computational complexity and machine model dependency, direct controllability of active and reactive powers, very good transitory response, and lower overall implementation complexity than field-oriented control scheme. It is also characterized by its fast-dynamic response against parameter variations and it does not utilize a rotor current control loop. The estimation of active and reactive powers is carried out using current measurements, and directly controlled with hysteresis controllers and a switching table. However, the frequency and voltage control are considered as open loop control. Thus, they need feedback signals to track the frequency and voltage fluctuations very quickly for damping accordingly. The parameters determined and used in the VSPS plant are listed in Appendix.

4.2. Control of RSC. Starting with the dynamics model of the three-phase induction machine based on the synchronous reference frame, the electrical equations of the DFIM are expressed by.

$$\begin{aligned}
\frac{d\Psi_{ds}}{dt} &= V_{ds} - R_s i_{ds} + \omega_s \Psi_{qs},\\
\frac{d\Psi_{qs}}{dt} &= V_{qs} - R_s i_{qs} - \omega_s \Psi_{ds},\\
\frac{d\Psi_{dr}}{dt} &= V_{dr} - R_r i_{dr} + (\omega_s - \omega_r)\Psi_{qr},\\
\frac{d\Psi_{ds}}{dt} &= V_{qr} - R_s i_{qr} - (\omega_s - \omega_r)\Psi_{dr},
\end{aligned} \tag{2}$$

$$\begin{aligned}
\Psi_{ds} &= L_s i_{ds} + L_m i_{dr},\\
\Psi_{qs} &= L_s i_{qs} + L_m i_{qr},\\
\Psi_{dr} &= L_s i_{dr} + L_m i_{ds},\\
\Psi_{qr} &= L_s i_{qr} + L_m i_{qs},\\
L_r &= L_{lr} + L_m,\\
L_s &= L_{ls} + L_m,
\end{aligned} \tag{3}$$

where; Ψ_{dqr}: dq-axis rotor fluxes, Ψ_{dqs}: dq-axis stator fluxes, i_{dqr}: dq-axis rotor currents, i_{dqs}: dq-axis stator currents, V_{dqs}: dq-axis stator voltages, V_{dqr}: dq-axis rotor voltages, L_m: magnetizing reactance, L_{lr}: rotor leakage reactance, L_{ls}: stator leakage reactance, R_r: rotor resistance, R_s: stator resistance, ω_r: electrical angular speed, ω_s: synchronous angular speed.

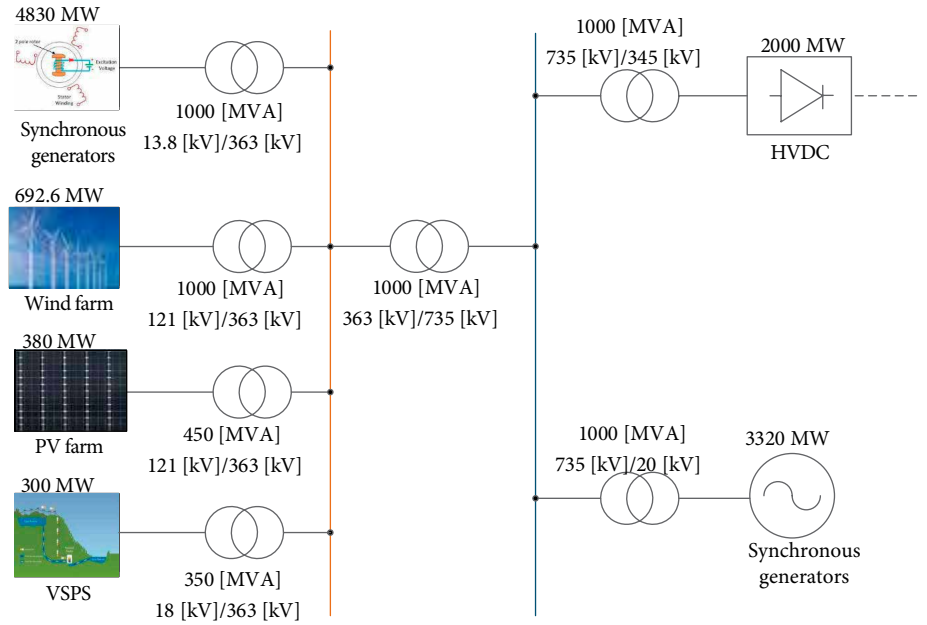

Figure 6: Structure of the proposed system to mitigate the effects of SSR in the power system.

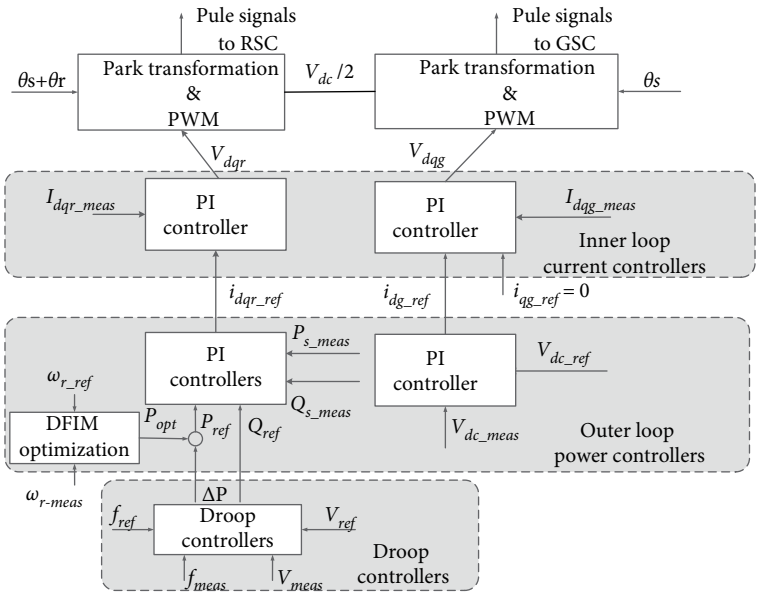

Figure 7: Overall structure of control strategy used in this paper implemented in the VSPS plant.

Based on [13], with the implementation of the vector control method, the stator flux is aligned with the d-axis. Taking the stator flux equations in (3), one can deduce that $\Psi_{qs} = 0$, and $\Psi_{ds} = \Psi_s$. Thus, from equations in (3), the following are obtained.

$$\begin{aligned} i_{ds} &= \frac{\Psi_s}{L_s} - \frac{L_m}{L_s} i_{dr}, \\ i_{qs} &= -\frac{L_m}{L_s} i_{qr}. \end{aligned} \tag{4}$$

Taking the assumption that the voltage drop across stator resistor is very small compared to the grid voltage, stator resistance can be neglected. Thus, $v_{ds} = 0$, and $v_{qs} = v_s$. Hence, substituting these and the values of $i_{qs} = 0$, and i_{ds} in (4) to (1), the following hold.

$$\begin{aligned} P_s &= \frac{3}{2} V_s \left(\frac{L_m}{L_s} \right) i_{qr}, \\ Q_s &= \frac{3}{2} V_s \left[\left(\frac{\Psi_s}{L_s} \right) - \left(\frac{L_m}{L_s} \right) i_{dr} \right]. \end{aligned} \tag{5}$$

Equation (5) explains that the active power and reactive power are independently controlled. This reveals that RSC offers a proper AC excitation for the windings of the rotor that provides the stator windings proper active power and used for controlling the turbine output power and the reactive power which is measured at the terminals of the stator of the machine

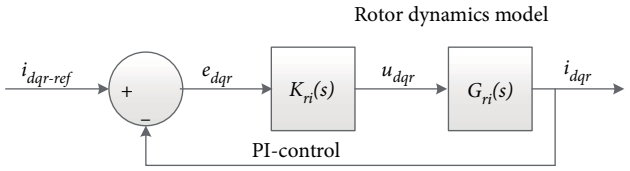

Figure 8: The PI current control (inner loop) structure of the RSC.

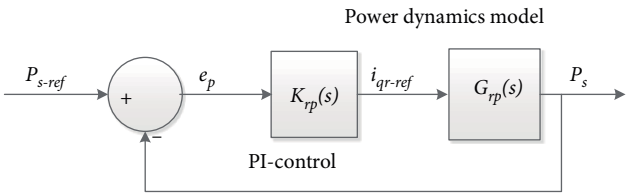

Figure 9: The PI active power control (outer loop) structure of the RSC.

[12]. The active power is regulated so as to follow a relationship of power and speed of the turbine of the DFIM.

The model used to control the currents is presented as under.

Taking the equation of (4) and differentiating the rotor flux leakage equation of the d-axis component with respect to time, the equation (6) holds.

$$\frac{d\Psi_{dr}}{dt} = L_r \frac{di_{dr}}{dt} + L_m \frac{di_{ds}}{dt}. \tag{6}$$

Substituting the derivative value of i_{qs} in (4) to (2), equation (7) is derived.

$$\frac{d\Psi_{dr}}{dt} = L_r \frac{di_{dr}}{dt} + L_m \frac{-L_m}{L_s} \frac{di_{ds}}{dt}. \tag{7}$$

Substituting the value of $d\Psi_{dr}/dt$ in (7) to the d-axis rotor equation of (2), equation (8) is derived.

$$V_{dr} = R_r i_{dr} + L_r^* \frac{di_{dr}}{dt} - (\omega_s - \omega_r)\left(L_r i_{qr} + L_m i_{qs}\right). \tag{8}$$

Following the same procedures to the q-axis, equation (9) holds.

$$V_{qr} = R_r i_{qr} + L_r^* \frac{di_{qr}}{dt} + (\omega_s - \omega_r)(L_r i_{dr} + L_m i_{ds}), \tag{9}$$

where $L_r^* = L_r - \left(L_m^2/L_s\right)$.

Equations of (8) and (9) are helpful to develop the inner current control loops. But, due to the presence of $L_r(\omega_s - \omega_r)$ terms in (8) and (9), the dynamics of i_{qr} and i_{dr} are coupled. To decouple the dynamics, one can determine m_{qr} and m_{dr}. Taking into account the theory of VSC, $mV_{dc}/2$ is the gain of the VSC. Thus, the computed signals V_{qr} and V_{dr} are divided by $V_{dc}/2$ to give, respectively, m_{qr} and m_{dr} signals. The modulated signals of m_{qr} and m_{dr} are defined by

$$\begin{aligned} m_{dr} &= \left(\frac{2}{V_{dc}}\right)\left[u_{dr} - (\omega_s - \omega_r)\left(L_r i_{qr} + L_m i_{qs}\right)\right], \\ m_{qr} &= \left(\frac{2}{V_{dc}}\right)\left[u_{qr} - (\omega_s - \omega_r)(L_r i_{dr} + L_m i_{ds})\right]. \end{aligned} \tag{10}$$

The two new control inputs are defined as

$$\begin{aligned} u_{dr} &= L_r^* \frac{di_{dr}}{dr} + R_r i_{dr}, \\ u_{qr} &= L_r^* \frac{di_{qr}}{dr} + R_r i_{qr}. \end{aligned} \tag{11}$$

Thus, the rotor electrical dynamics model is determined and representing two decoupled, first-order subsystems.

The plant transfer function is given by

$$G_{ri}(s) = \frac{I_{dqr}(s)}{U_{dqr}(s)} = \frac{1}{L_r^* s + R_r}. \tag{12}$$

These subsystems are the rotor-current control loops. Feedforward terms predicting V_{qr} and V_{dr} are provided on both inner loops. The loops can now control i_{qr} and i_{dr} with the PI compensators. The PI compensator with k_p^{ri} as proportional gain and k_i^{ri} as integral gain of the compensator is defined by

$$K_{ri}(s) = \frac{k_p^{ri} s + k_i^{ri}}{s}. \tag{13}$$

Based on these mathematical models of (12) and (13), the control structure is built and illustrated in Figure 8.

The outer loops are developed to generate the reference current $i_{dqr-ref}$ to the inner loops. From Figure 8, the closed loop transfer function of q-axis current can be defined by

$$i_{qr}(s) = \frac{K_{ri} G_{ri}}{1 + K_{ri} G_{ri}} i_{qr-ref}(s). \tag{14}$$

Based on (5) and substituting the value of $i_{qr}(s)$ in (14) to it (5), the active power is expressed by (15).

$$P_s = \frac{3}{2} \frac{L_m}{L_s} V_s \frac{K_{ri} G_{ri}}{1 + K_{ri} G_{ri}} i_{qr-ref}(s) = G_{rp}(s) i_{qr-ref}(s). \tag{15}$$

Therefore, the plant function of active power in (15) can be controlled by PI compensator. The control structure is shown in Figure 9.

Where the PI-control is denoted by.

$$K_{rp}(s) = \frac{k_p^{rp} s + k_i^{rp}}{s}, \tag{16}$$

with k_p^{rp} and k_i^{rp} are, respectively, proportional and integral gains of the controller. The refence value of P_{s-ref} is determined from the optimization of the hydraulic turbine.

Moreover, controlling of active power can ensure controlling of grid frequency. But, in the above model, frequency is controlled in a mode of open loop scheme. Thus, the frequency could not be fully regulated and leads to more excursions. Hence, the frequency needs to be designed in such a way that the frequency closed loop circuit is added to the above active power control loop as a concept of droop control. The droop control can compensate if some excursions of a grid frequency occur due to contingencies including SSR. The control structure is illustrated in (Figure 10). The droop constant K_f is computed by (17).

$$K_f = \frac{-\Delta f/f}{\Delta P/P}, \tag{17}$$

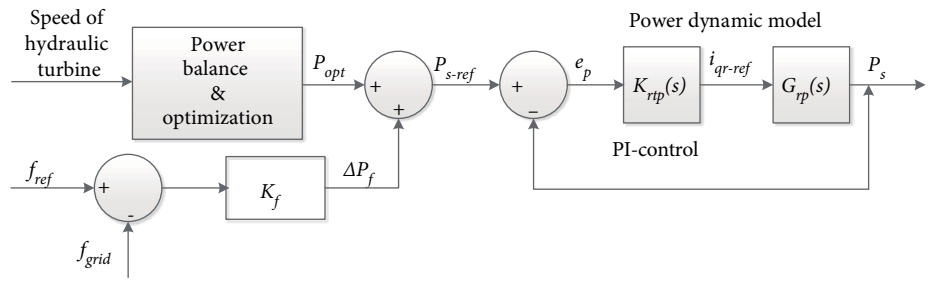

Figure 10: Droop-based direct power vector control structure for RSC of the VSPS (active power control loop).

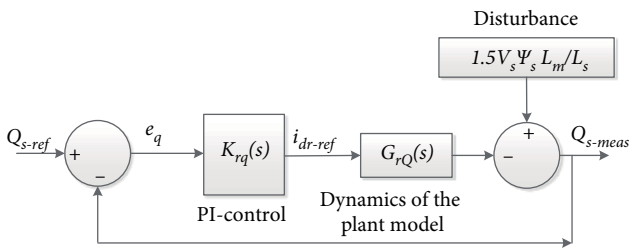

Figure 11: The PI reactive power control loop structure of the RSC.

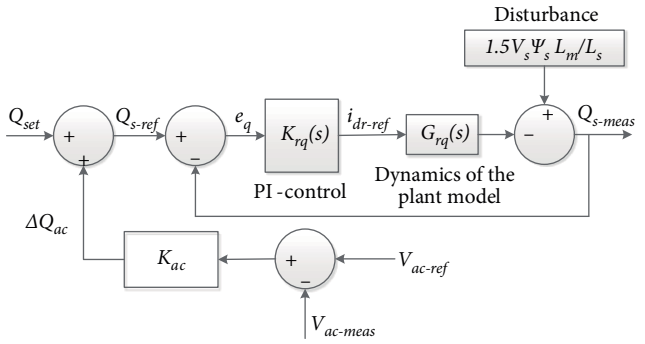

Figure 12: Droop-based direct power vector control structure for RSC of the VSPS (reactive power control loop).

where, Δf is allowable deviation of grid frequency, ΔP is and P is the maximum power carried by the converter.

The reactive power control design is presented as follow. From (5) and Figure 8, the equation (18) holds.

$$\begin{aligned} P_s &= -\frac{3}{2}\frac{L_m}{L_s}V_s\frac{K_{ri}G_{ri}}{1+K_{ri}G_{ri}}i_{dr-ref}(s)+\frac{3}{2}\frac{\Psi_s}{L_s} \\ V_s &= G_{rQ}(s)i_{qr-ref}(s)+\frac{3}{2}\frac{\Psi_s}{L_s}V_s. \end{aligned} \tag{18}$$

Thus, the dynamics of (18) can be controlled by applying PI control and the control structure is depicted in Figure 11.

In this model, the AC voltage is controlled through controlling reactive power but the reference of reactive is set to a fixed value. This leads to deviations and instability when contingencies occur. The reference value of the reactive value should be determined through the proportional value of change of AC voltage. This process is effective by providing the droop control loop to add with the above reactive power control loop. The control structure of this new idea is shown in the Figure 12.

The constant of the droop loop is determined based on the concept emerged from Figure 13.

From Figure 13, we can have (19).

$$\begin{aligned} V_{t-SG} &= e_{SG}+k_{SG}(R_{SG}+jX_{SG})i_{SG}, \\ V_{t-SG} &= e_{SG}+k_{SG}(R_{SG}+jX_{SG})i_{SG}. \end{aligned} \tag{19}$$

Equation (19) states that with the voltage control units connected in parallel, the load compensation is likely made.

4.3. Control of GSC. The objective of the active/reactive power controller of the VSC system is to regulate the active/reactive power exchange between the converter and the AC grid. Active

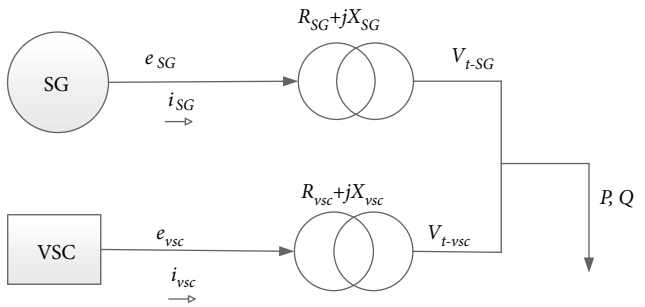

Figure 13: Block diagram of voltage-control units connected in parallel for briefing voltage droop control.

power is controlled by controlling the DC voltage that ensures the converter operation at unity power factor. The VSC based model also allows the GSC to absorb or generate reactive power. So, since there is no reactive power exchange initially, the reactive power control can be handled only by inner loop of current control. The control design is presented in the following.

Based on Figure 14, the voltage equations across the coupling inductor in dq-frame are determined. The same procedure as done in the RSC is followed for developing the inner loops (current controllers). The equations are expressed by

$$V_{dg} = Ri_{ds}+L\frac{di_{ds}}{dt}-\omega_s Li_{qs}+V_{ds}, \tag{20}$$

$$V_{qg} = Ri_{qs}+L\frac{di_{qs}}{dt}-\omega_s Li_{ds}+V_{qs}, \tag{21}$$

where R and L are resistance and inductance of the coupling inductor.

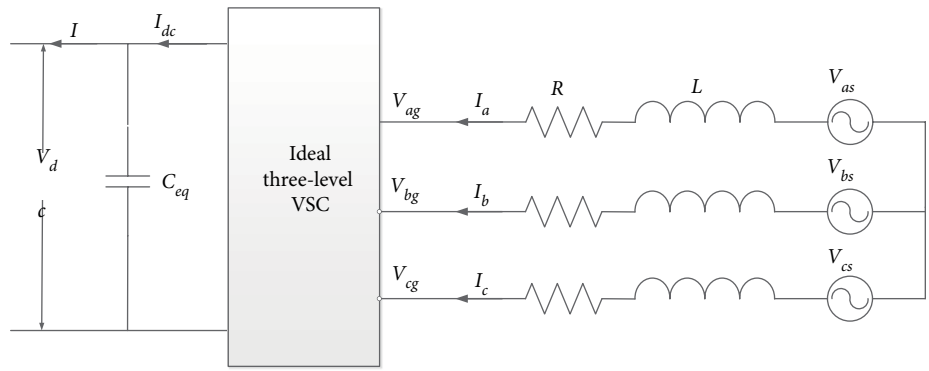

Figure 14: A simplified GSC equivalent circuit.

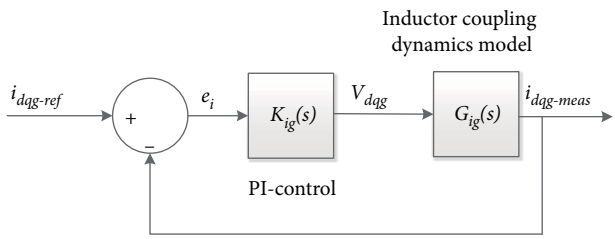

Figure 15: The control structure for the GSC current control (inner loops).

To decouple the dynamics of i_{dg} and i_{qg}, the modulated signals of m_{dg} and m_{qg} are determined as.

$$m_{dg} = \left(\frac{2}{V_{dc}}\right)\left[u_{dg} - \omega_s\left(Li_{qg} + L_m i_{qs}\right)\right], \tag{22}$$

$$m_{dg} = \left(\frac{2}{V_{dc}}\right)\left[u_{dg} - \omega_s\left(Li_{qg} + L_m i_{qs}\right)\right]. \tag{23}$$

Thus, the two new control inputs for the inner current loops are defined in (24) and (25) and supported by feed forward terms predicting V_{dg} and V_{qg}.

$$u_{dg} = L\frac{di_{dg}}{dt} + Ri_{dg}, \tag{24}$$

$$u_{qg} = L\frac{di_{qg}}{dt} + Ri_{qg}. \tag{25}$$

The compensator can be a simple proportional-integral (PI) compensator, $K_{gi}(s)$ to enable tracking of a respective reference signal. The compensator is defined by

$$K_{gi}(s) = \frac{k_p^{gi}s + k_i^{gi}}{s}. \tag{26}$$

Thus, based on the plant function, $G_{gi}(s) = 1/(Ls + R)$ and considering the compensator $K_{gi}(s)$ in (26), the closed-loop desired transfer function becomes

$$\frac{I_{dqg}(s)}{I_{dqg-ref}(s)} = G_{gi}(s) = \frac{1}{\tau_{gi}s + 1}, \tag{27}$$

if and only if $k_p^{gi} = L/\tau_{gi}$ and $k_i^{gi} = R/\tau_{gi}$.

Where k_p^{gi} and k_p^{gi} are proportional and integral gains. The gains are determined and then tuned based on the control stability theory until the better result is achieved. The control loop is illustrated in Figure 15.

The d-axis is, for control design purposes, supposed to be set in phase with the voltage across the resistor, and neglecting the harmonics and losses due to switching in the converter, the active power balance equation is given by:

$$\begin{aligned} V_{dc}I_{dc} &= 1.5v_{dg}i_{dg} = P_r, \\ \because v_{qg} &= 0, \end{aligned} \tag{28}$$

and on the output side, the dc current is

$$I_{dc} = C\frac{dv_{dc}}{dt} + i_L, \tag{29}$$

where V_{dc} and I_{dc} are dc output voltage and current respectively.

Thus, the d-component of the voltages in $d-q$ coordinates becomes v_{dg} and zero that of v_{qg}. So, the active and reactive power equations are deduced by (30) and (31) respectively.

$$P_g = 1.5v_{dg}i_{dg}, \tag{30}$$

$$Q_g = -1.5v_{dg}i_{qg}. \tag{31}$$

These equations prevail that active power is likely controlled by i_{dg} and reactive power by i_{qg}. Based on (32), the real power balance equation on the grid side can be given by:

$$P_g = 1.5v_{dg}i_{qg} = V_{dc}I_{dc}. \tag{32}$$

Equation (32) implies that the active power can be controlled by controlling the DC-bus voltage and in such a way that independently the DC voltage is controlled by controlling the d-axis current i_{dg}. In this controller, for the sake of mathematical formulation, it is supposed to be the DC side of the VSC is connected to an ideal DC voltage source that dictates the DC-bus voltage as shown in Figure 14. Thus, the DC-voltage V_{dc} of the grid port requires proper regulation.

The current controller as described earlier is ensured that the output current tracks the reference values generated by an additional external control loop, which performs the output active power regulation. This power regulation is confirmed by implementing the dc voltage control. The DC link dynamics of Figure 14 is given by

$$C\frac{dv_{dc}}{dt} = \frac{3}{2}\frac{V_{dg}}{V_{dc}}i_{dg} - i_L. \tag{33}$$

The minimum value of required DC side voltage [15] is given by the inverter output voltage as,

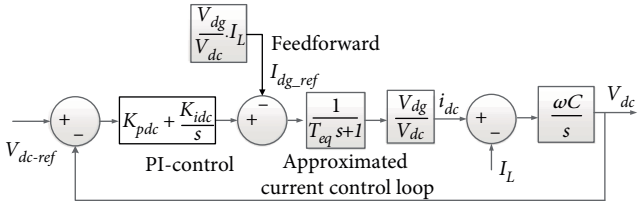

Figure 16: The control structure of the DC voltage control of the DC link in the VSCs.

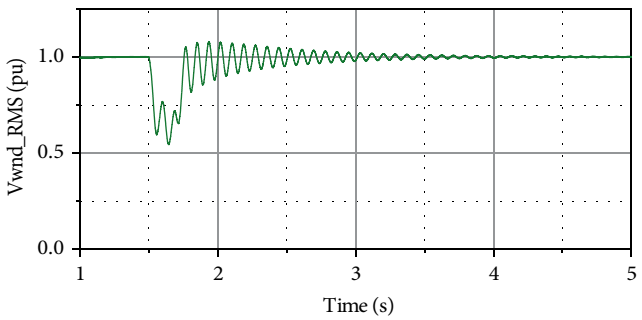

Figure 17: Voltage characteristics on the machine terminal voltage of the wind farm.

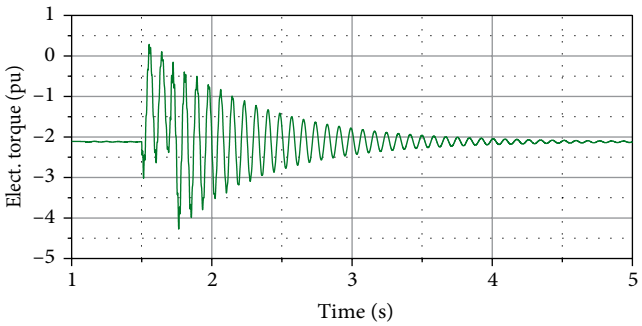

Figure 18: The electrical torque characteristics of the wind farm.

$$V_{dc} = 2\sqrt{\frac{2}{3}}\, V_{LL,rms} = 2V_{peak,ph}. \tag{34}$$

where $V_{peak,ph}$ is peak phase voltage at the ac side and $V_{LL,rms}$ is the line-line *rms* voltage.

Since the DC-link dynamics of (33) is a nonlinear equation, the PI control parameters are to be determined by linearizing the operating point of the system model. For linearization of the system model, the input value V_{dc-ref} is specified as a reference and it yields the transfer function as.

$$\frac{\Delta V_{dc}(s)}{\Delta i_{dg}(s)} = \frac{3}{2}\frac{V_{dg,0}}{V_{dc-\mathrm{ref}}}\frac{1}{sC}. \tag{35}$$

To analyse this control loop, the inner current control closed loop is approximately defined as first order system with time constant T_{eq} which is about to be $2T_a$ [14]. T_a is the time constant of the inner current loop plant function. Thus, the control structure of the DC voltage control is depicted in (Figure 16).

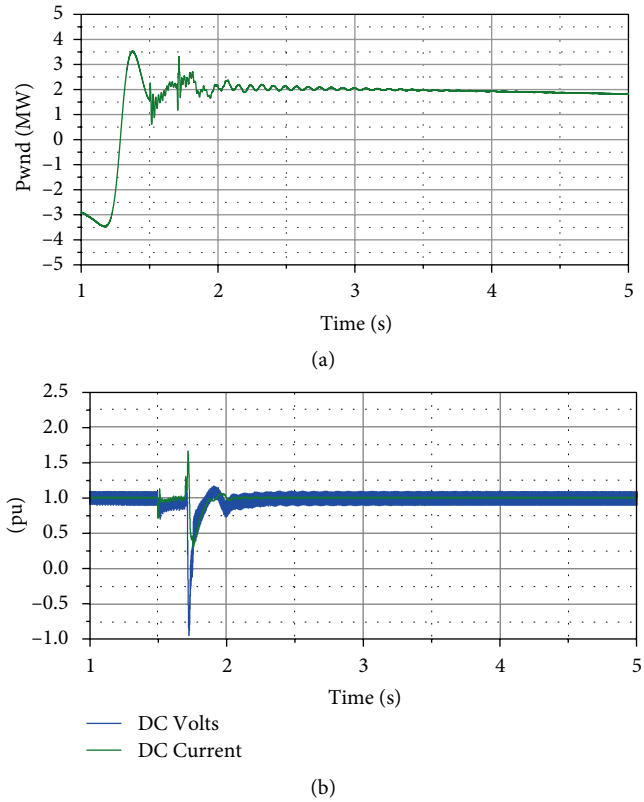

Figure 19: Evolution of the proposed network to demonstrate the SSR effect reduction on. (a) Power flow characteristics in the wind farm. (b) DC voltage and current response in the HVDC.

The capacitor current in dc link is controlled by the DC voltage controller to maintain the power balance between the grid and the converter. Thus, in balanced conditions, $i_c = 0$ and $I_{dc} = I_L$. Hence, the current reference value of I_{dg} should ensure exact compensation for load variation. The complete block diagram of dc-link voltage controller is represented as in Figure 10 as the system equations are analysed in per unit [14], where K_{pdc} and K_{idc} are PI controller parameters, and C is per unit capacitance of DC link.

The load variation can be greatly reduced if feed-forward method is used. Otherwise, to reduce the large error, the large gain of voltage controller which is important from stability viewpoint is not necessarily deployed.

5. Simulation Results and Discussion

Figures 17–19 show the responses of the proposed system and the analysis is compared with the simulated results presented in chapter two. The time duration for the case study is set as the same duration as the above discussion and description shown in Figures 3–5. This is for arguing and verifying the hypothesis of the proposed system.

Figures 17 and 18 show the response of machine terminal voltage and torque characteristics where the SSR model is in effect on the wind farm. Comparing with the responses shown in Figure 5, the oscillations in the torque characteristics are significantly reduced. This is because the control strategy designed on the VSPS is capable of balancing the mismatch

Table 1: The parameters of the VSPS.

Type of the parameter	Unit	Value
Turbine rating	MW	300
Rated hydraulic head	m	165
Piping area	m^2	11.15
Gate opening at no load	pu	0.06
Gate opening at full load	pu	0.94
Generator power capacity	MVA	333
Generator terminal voltage	kV	18
Base value of the power	MVA	333
Base value of the voltage	kV	220
Stator resistance	pu	0.0086
Stator leakage inductance	pu	0.152
Rotor resistance	pu	0.007
Rotor leakage inductance	pu	0.187
Magnetization inductance	pu	300
Inertia constant	Sec.	10.6
Friction coefficient	pu	0.02
Pairs of poles	No.	12
Converter rating	MVA	66
Converter DC-link voltage	kV	38
DC-link equivalent capacitance	mF	20
The coupling inductor resistance	pu	0.0025
The coupling inductor inductance	pu	0.25
The rotor side controller		
Current loop proportional gain	k_p^{ri}	1.25
Current loop integral gain	k_i^{ri}	15
Active power loop proportional gain	k_p^{rp}	1.5
Active power loop integral gain	k_i^{rp}	20
Reactive power loop proportional gain	k_p^{rq}	0.3
Reactive power loop integral gain	k_i^{rq}	5.5
Frequency droop constant	K_f	30
AC voltage droop constant	K_{AC}	60
The grid side controller		
Current loop proportional gain	k_p^{gi}	1.1
Current loop integral gain	k_i^{gi}	9
DC voltage loop proportional gain	K_{pdc}	0.001
DC voltage loop integral gain	K_{idc}	0.02
Grid connecting transformer		
Power capacity	MVA	350
Voltage transformation ratio	unitless	18/363
primary winding resistance	pu	0.0025
Secondary winding resistance	pu	0.0025
Primary winding inductance	pu	0.08
Secondary winding inductance	pu	0.08
Magnetization resistance	pu	500
Magnetization inductance	pu	500

power between the shaft power and electromagnetic power and in turn to reduce the torque oscillations and the regulated electromagnetic power to cancel the effect of shaft torque resonance interaction with series capacitor.

The voltage responses become improved from the oscillations due to SSR. It is the reason that the SSR is compensated by the VSPS reactive power control strategy. The VSPS is capable of generating and absorbing the reactive power and hence regulating the AC voltage oscillations based on the required and given reference voltage value using the AC droop controller.

Additionally, because of the SSR effects on the system frequency and power flow, the effects were elongated on the power flow in to HVDC system. However, due to the SSR reduction by the VSPS with its control strategy, the oscillation effects on the wind farm, HVDC and synchronous hydropower plant are being minimal. These results are shown in Figure 19.

6. Conclusion

This paper presents a study on the mitigation method of SSR in the power system using VSPS plant. This new method is deployed to mitigate the effects of SSR with the implementation of VSPS plant based on the principle of balanced shaft mechanical input power and electromagnetic power of the VSPS. The droop-based direct power control strategy on the bases of dq-coordinate technique is designed. For the sake of implementation, IEEE second benchmark model is used and its effect by simulation with the PSCAD platform discussed. A case of Ningxia power grid area is taken for the realization of the proposed system.

The results show that the proposed VSPS system along with its appropriate control strategy achieves well-regulated power flow and AC voltage so as to reduce the effects of SSR spreading in the power system. Hence, VSPS plant ensures to mitigate SSR which causes instability and security problem in the power grid.

Appendix

Table 1 includes the parameters of the VSPS in the proposed system studied in this paper.

Data Availability

The data used to support the findings of this study are included within the article.

Conflicts of Interest

The authors declare that they have no conflicts of interest.

Funding

This research is supported by the project assigned by State Grid Ningxia Electric Power Co., Ltd.

References

[1] R. Rajaraman and I. Dobson, "Justification of torque per unit velocity methods of analyzing subsynchronous resonance and a swing mode in power systems," *IEEE Transactions on Circuits and Systems I: Fundamental Theory and Applications*, vol. 45, no. 10, pp. 1109–1113, 1998.

[2] N. Johansson, L. Ängquist, and H. P. Nee, "A comparison of different frequency scanning methods for study of

subsynchronous resonance," *IEEE Transactions on Power Systems*, vol. 26, no. 1, pp. 356–363, 2011.

[3] M. Ghafouri, U. Karaagac, H. Karimi, S. Jensen, J. Mahseredjian, and S. O. Faried, "An LQR controller for damping of subsynchronous interaction in DFIG-based wind farms," *IEEE Transactions on Power Systems*, vol. 32, no. 6, pp. 4934–4942, 2017.

[4] C. Zhu, L. Fan, and M. Hu, "Control and analysis of DFIG-based wind turbines in a series compensated network for SSR damping," in *IEEE PES General Meeting, PES*, IEEEProvidence, RI, USA, 2010.

[5] U. Karaagac, S. O. Faried, J. Mahseredjian, and A. A. Edris, "Coordinated control of wind energy conversion systems for mitigating subsynchronous interaction in DFIG-based wind farms," *IEEE Transactions on Smart Grid*, vol. 5, no. 5, pp. 2440–2449, 2014.

[6] X. Xie, X. Zhang, H. Liu, H. Liu, Y. Li, and C. Zhang, "Characteristic analysis of subsynchronous resonance in practical wind farms connected to series-compensated transmissions," *IEEE Transactions on Energy Conversion*, vol. 32, no. 3, pp. 1117–1126, 2017.

[7] L. Yunhong, L. Hui, C. Xiaowei, H. Jing, and Y. Li, "Impact of PMSG on SSR of DFIGs connected to series-compensated lines based on the impedance characteristics," *The Journal of Engineering*, vol. 2017, no. 13, pp. 2184–2187, 2017.

[8] M. Pöller and S. Achilles, "Aggregated wind park models for analyzing power system dynamics," *Wind Engineering*, 2003.

[9] L. M. Fernández, F. Jurado, and J. R. Saenz, "Aggregated dynamic model for wind farms with doubly fed induction generator wind," *Renewable Energy*, vol. 33, no. 1, pp. 129–140, 2008.

[10] N. W. Miller, J. J. Sanchez-Gasca, W. W. Price, and R. W. Delmerico, "Dynamic modeling of GE 1.5 and 3.6 MW wind turbine-generators for stability simulations2003," in *IEEE Power Engineering Society General Meeting (IEEE Cat. No.03CH37491)*, IEEE, Toronto, Ont., Canada, 2004.

[11] R. Piwko, N. Miller, J. Sanchez-Gasca, X. Yuan, R. Dai, and J. Lyons, "Integrating large wind farms into weak power grids with long transmission lines," in *Conference Proceedings – IPEMC 2006: CES/IEEE 5th International Power Electronics and Motion Control Conference*, IEEE, Dalian, China, 2007.

[12] G. Bitew, M. Han, S. Mekonnen, and P. Simiyu, "A variable speed pumped storage system based on droop-fed vector control strategy for grid frequency and AC-bus voltage stability," *Electronics*, vol. 7, no. 7, p. 108, 2018.

[13] U. Nasir, I. Student, and Z. Iqbal, "Active and reactive power control of a variable speed pumped storage system," in *2015 IEEE 15th International Conference on Environment and Electrical Engineering (EEEIC)*, IEEE, pp. 6–11, Rome, Italy, 2015.

[14] T. Jacob, "Pumped storage in Switzerland: outlook beyond 2000," *International Journal on Hydropower and Dams*, 1997.

[15] C. Wei, M. Benosman, and T. Kim, "Online parameter identification for state of power prediction of lithium-ion batteries in electric vehicles using extremum seeking," *International Journal of Control, Automation and Systems*, pp. 1–11, 2019.

[16] F. Cheng, L. Qu, W. Qiao, C. Wei, and L. Hao, "Fault diagnosis of wind turbine gearboxes based on DFIG stator current envelope analysis," *IEEE Transactions on Sustainable Energy*, vol. 10, no. 3, pp. 1044–1053, 2019.